nature materials

SUPPLEMENTARY INFORMATION

DOI: 10.1038/NMAT4276

Quasiparticle-mediated spin Hall effect in a superconductor

T. Wakamura[1], H. Akaike[2], Y. Omori[1], Y. Niimi[1], S. Takahashi[3], A. Fujimaki[2], S. Maekawa[4,5] and YoshiChika Otani[1,6]

[1]*Institute for Solid State Physics, University of Tokyo, Kashiwa 277-8581, Japan*

[2]*Department of Quantum Engineering, Nagoya University, Nagoya 464-8603, Japan*

[3]*Institute for Materials Research, Tohoku University, Sendai 980-8577, Japan*

[4]*CREST, Japan Science and Technology, Tokyo 102-0075, Japan*

[5]*Advanced Science Research Center, Japan Atomic Energy Agency, Tokai 319-1195, Japan and*

[6]*RIKEN-CEMS, 2-1 Hirosawa, Wako, Saitama 351-0198, Japan*

(Dated: February 4, 2015)

DOI: 10.1038/NMAT4276

S.1 DETAILS OF THE DEVICES

In this section we show the details of the device structure and measurements. Figure 1(a) displays the SEM image of a device. The center-to-center distance between the Py spin injector and the NbN wire is 450 nm. In Fig. 1(b), we show the temperature dependence of resistance of the NbN wire. The coherence length ξ of the NbN wire is estimated to be $\xi =$ 4 nm using the relation

$$\xi = \sqrt{\frac{\hbar D}{\Delta_0}}, \tag{1}$$

where the superconducting gap at $T = 0$, Δ_0 is related to T_C as $\Delta_0 = 2.2 k_B T_C$ for a strong coupling superconductor, NbN [31]. We note that the inplane critical field of the NbN wire is larger than ~ 1 T, a maximum field applicable in our system.

S.2 SPIN HALL EFFECT OF NBN ABOVE T_C

The spin Hall effect (SHE) is a nonmagnetic counterpart of the anomalous Hall effect (AHE), which occurs in ferromagnets and has been investigated for many decades. Previous findings for the AHE are also applicable to the SHE; the SHE is attributed to an intrinsic effect and extrinsic effects. The intrinsic effect was first pointed out by Karplus and Luttinger [32] in the concept of the anomalous velocity, and arises from the band structure of perfect

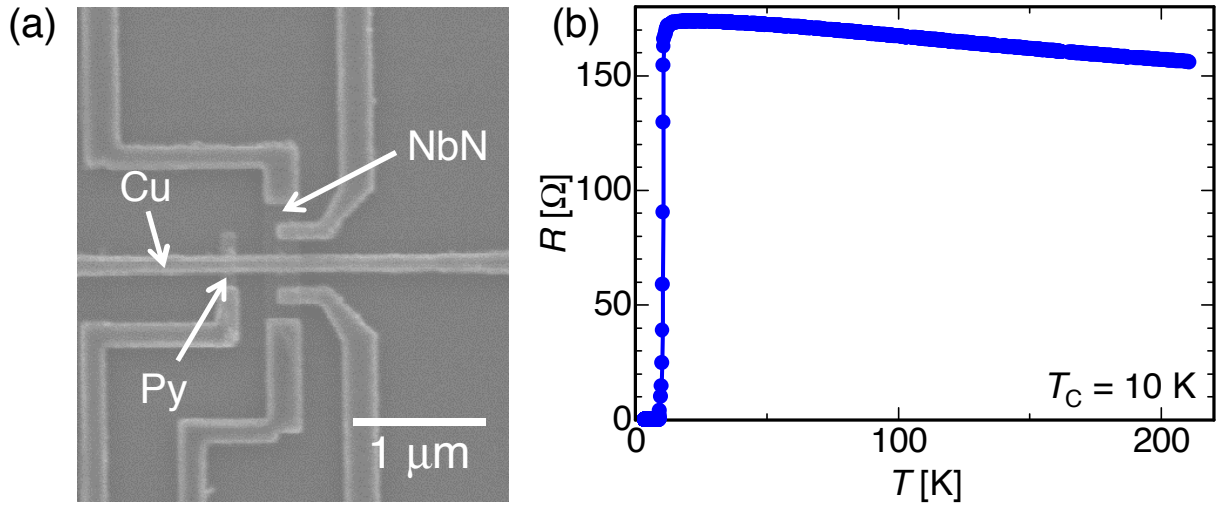

FIG. 1. (a): SEM image of a device. (b): Resistance of the NbN wire (R) as a function of temperatuire (T).

crystals. It is characterized by a finite value of an integrated Berry phase curvature in the momentum space [33]. Previous studies on the AHE demonstrate that when the intrisic effect is dominant, the relation between the Hall resistivity ρ_{yx} (or the spin Hall resistivity $\rho_{\rm SHE}$ in the SHE) and the longitudinal resistivity ρ_{xx} is $\rho_{yx} \propto \rho_{xx}^2$ in moderately resistive metals [34]. The extrinsic effects are, on the other hand, relevant to disorder scatterings in imperfect crystals. There are two contributions to the extrinsic effects; the skew-scattering (SS) [35] and the side-jump (SJ) [36] effect. The SS contribution arises from spin-asymmetric scatterings by impurities with strong spin-orbit interaction. When the SS is dominant, one obtains the relation $\rho_{yx} \propto \rho_{xx}$. The SJ effect brings the anomalous velocity to electrons thus the electrons move transversely when scattered. In this regime $\rho_{yx} \propto \rho_{xx}^2$. Taking these three contributions into account, ρ_{yx} can be expressed as

$$\rho_{yx} = a\rho_{xx} + b\rho_{xx}^2, \tag{2}$$

where both a and b are constant. We note that we follow the conventional relation between ρ_{yx} and ρ_{xx} in (2) and do not replace ρ_{xx} with $\rho_{\rm imp}$ for the extrinsic contributions as done in [37], where $\rho_{\rm imp}$ is a temperature independent impurity resistivity. This is because in our system we cannot explicitly distinguish the extrinsic effects from the intrinsic effect. The Hall angle (or the spin Hall angle), defined as $\alpha_{\rm H}(\alpha_{\rm SHE}) \equiv \rho_{yx}(\rho_{\rm SHE})/\rho_{xx}$, is thus written as

$$\alpha_{\rm H} = a + b\rho_{xx}. \tag{3}$$

As shown in Fig. 1(b), above $T_{\rm C}$(=10 K) one can see the linear relation between R (namely, ρ_{xx}) and T. In the main part of our paper we show that the spin Hall angle $\alpha_{\rm SHE}$ is proportional to T. Thus by using these two relations we can determine two constants a and b.

S.3 RELATION BETWEEN THE SPIN INJECTION CURRENT I AND THE EFFECTIVE TEMPERATURE AT THE CU/NBN INTERFACE

In order to confirm that superconductivity is sustained in the NbN wire close to the interface with the Cu bridge, we measured the temperature (T) dependence and spin injection current (I) dependence of the resistance of the NbN. The results are shown in Fig. 2 with the measurement setup in the inset. $R_{\rm I}$ is defined as V/i ($V \equiv (V_+ - V_-)$) with i the

DOI: 10.1038/NMAT4276

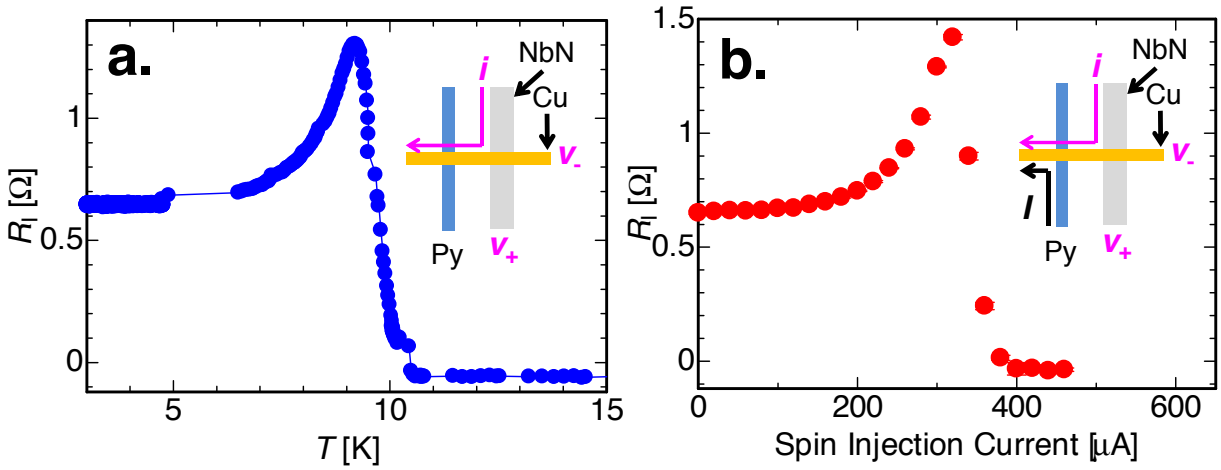

FIG. 2. **a.** Temperature dependence of the interface resistance $R_{\mathrm{I}} \equiv V/i$, $V = V_+ - V_-$. **b.** Spin injection current (I) dependence of R_{I}. Insets show the measurement setup.

bias current. As for the temperature dependence, when $T > T_{\mathrm{C}}$, $R_{\mathrm{I}} < 0$, originated from current inhomogeneities at the transparent Cu/NbN interface [38, 39]. At $T = T_{\mathrm{C}}$, a peak structure appears, and extra resistance is added for $T < T_{\mathrm{C}}$ (Fig. 2a). They originate from the charge imbalance effect, a nonequilibrium phenomenon relevant to superconductivity of the NbN, as observed in the previous studies [40, 43]. When we fixed T and modulating I, we obtained exactly the same curve as the temperature dependence of R_{I} (Fig. 2b). In our previous work [40], we observed the same correspondance between T and I dependence of the resistance close to the superconductor/normal metal interface, and by comparing these two curves, we can estimate the effective temperature at the superconductor/normal metal interface for a certain I. In this study, we can also apply the same way to evaluate the effective temperature at the Cu/NbN interface, which is modulated through I.

To acquire the relation between I and the effective temperature it is necessary to consider the Wiedemann-Franz law and determine temperatures for electrons, phonons and the substrate, and also the coupling constants among them as discussed in [41]. We estimated the temperature difference in the Cu bridge between the Py spin injector and the NbN wire based on the Wiedemann-Franz law, and found that the temperature difference is negligibly small (< 0.1 K). We next evaluate the temperature difference between electrons and phonons. We note here that our measurements are performed above 3 K. As many previous studies on the temperature dependence of the phase coherence time in metals revealed [42], from 3 K and above the dephasing due to the electron-phonon coupling becomes more important

than that due to the electron-electron interaction. Therefore the phonon temperature cannot be decoupled from the electron temperature, indicating that the same temperature for electrons and phonons can be assumed. As for the thermal coupling between the substrate and phonons, the Kapitza resistance becomes significant at low temperatures as pointed out in [41]. However, in the present case measurements are done at much higher temperatures than those in [41], thus the Kapitza resistance is not so critical.

Taking into accout these facts, to calculate the relation between I and the effective temperature, we used a simple model. We first consider the temperature dependence of the energy density per unit volume, which is obtained by integrating the temperature dependence of the heat capacity of a material, as

$$\varepsilon = \gamma T^2 + AT^4, \tag{4}$$

where γ is the electronic heat capacity and A is the heat capacity of phonons [45]. We assume here that the electronic temperature and the phonon temperature are the same ($=T$) based on the above considerations. As a heat source, we assume that main contribution is from the Py wire, which has much larger resistance than that of the Cu wire. When a current I flows in a wire with a resistance R for time t, we have the Joule heating thus thermal energy is

$$Q = RI^2t, \tag{5}$$

where R is the resistance of the Py and t is the duration for electrons to pass through the Py wire. Taking into account the diffusive transport, t can be written as

$$t = \frac{L_{\mathrm{Py}}^2}{D}, \tag{6}$$

with the diffusion constant D of Py and the length L_{Py} of the Py spin injector (in the present case $L_{\mathrm{Py}} = 90$ nm). D is estimated to be $D = 2.0$ cm^{2}s^{-1} by using the Einstein's relation $\sigma = e^2N(0)D$ with the conductivity of Py $\sigma = 5 \times 10^6\ \Omega^{-1}\mathrm{m}^{-1}$ and the density of the states at the Fermi energy $N(0) = 1.0 \times 10^{48}$ J^{-1} m^{-3} [44]. Associating Eq. (5) with the net increase of the energy density:

$$\Delta\varepsilon = \gamma(T^2 - T_0^2) + A(T^4 - T_0^4), \tag{7}$$

where T_0 is the enviromental temperature, then we can write

$$I^2 = \frac{\gamma V}{Rt}(T^2 - T_0^2) + \frac{AV}{Rt}(T^4 - T_0^4), \tag{8}$$

DOI: 10.1038/NMAT4276

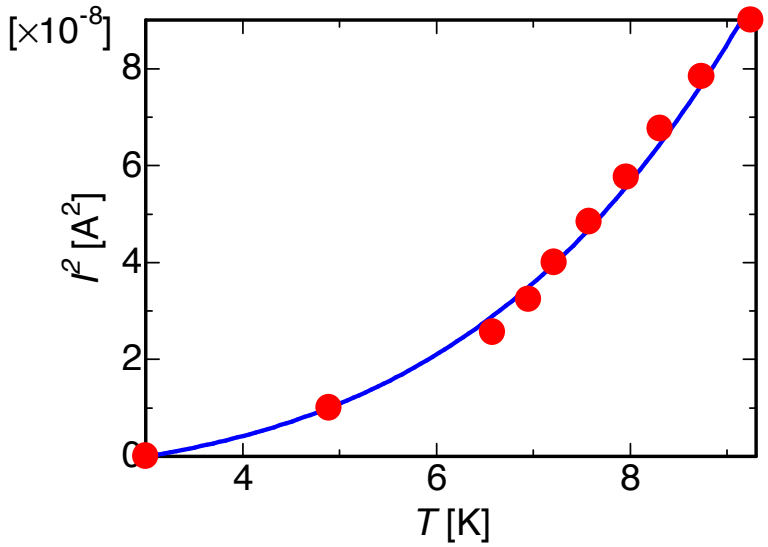

FIG. 3. I^2 as a function of T from the experimental results with the fitting curve calculated based on (8).

where V is the volume of the Cu bridge which mediates the heat flow. We show in Fig. 3 the experimental results on the relation between I^2 and the effective temperature with the fitting curve based on the equation (8). The curve reproduces the experimetal data fairly well, and we can obtain $\gamma = 64$ J-m^{-3}-K^{-2} and $A = 5.1$ J-m^{-3}-K^{-4}. These values are very close to the value from the reference $\gamma = 94$ J-m^{-3}-K^{-2} and $A = 8.7$ J-m^{-3}-K^{-4} [45], indicating the validity of our model to estimate the effective temperature at the Cu/NbN interface. By using this method we can determine T for each I. In the next section we discuss the details of the calculations for the inverse spin Hall signals considering this relation between T and I.

S.4 DETAILS OF THE CALCULATION FOR THE ABSORBED SPIN CURRENT INTO THE NBN

In order to reproduce the enormous enhancement of the inverse spin Hall signals below $T_{\rm C}$, we show the details of the calculation which relates the superconductivity of the NbN to the SHE. From the previous studies, the relation between the spin Hall resistivity $\rho_{\rm SHE}$ and the inverse spin Hall signal within the one-dimensional model is expressed as [46]

$$\rho_{\rm SHE} = \frac{w_{\rm M}}{\zeta}\left(\frac{I}{I_{\rm s}}\right)\Delta R_{\rm ISHE}, \tag{9}$$

where $w_{\rm M}$, ζ and $I_{\rm s}$ represent the width of the NbN wire, a shunting factor and a spin current injected into the NbN wire, respectively [46].

As discussed in S.1, $\rho_{\rm SHE}$ is expressed with ρ_{xx} as

$$\rho_{\rm SHE} = a\rho_{xx} + b\rho_{xx}^2. \tag{10}$$

It is important to note that in the superconducting state it is necessary to replace ρ_{xx} to $\rho_{\rm qp}$, the resistivity of quasiparticles. In the theoretical studies it is found that $\rho_{\rm qp}$ can be expressed with ρ_{xx} as $\rho_{\rm qp} = \rho_{xx}/[2f_0(\Delta)]$, where $f_0(\Delta) = (\exp(\Delta/k_{\rm B}T) + 1)^{-1}$ is the Fermi distribution function at the superconducting gap Δ of the NbN [47]. Then from (9) and (10), we obtain

$$\Delta R_{\rm ISHE} = \left(\frac{I_{\rm s}}{I}\right)\frac{\zeta}{w_{\rm M}}\left(a\frac{\rho_{xx}}{2f_0(\Delta)} + b\left(\frac{\rho_{xx}}{2f_0(\Delta)}\right)^2\right)e^{-\frac{d}{\lambda_{\rm Q}}}. \tag{11}$$

In the above equation effects from superconductivity are taken into account via $f_0(\Delta)$. Since the ISHE is observed via the charge imbalance effect, the measured signals are dependent on the distance between the voltage probe and the Cu/NbN junction. To take this into account, we include the decay of the charge imbalance effect with a factor $e^{-\frac{d}{\lambda_{\rm Q}}}$, where $\lambda_{\rm Q}$ is the charge imbalance length and d is the distance between the Cu/NbN junction and the edge of the NbN wire. Due to the transparent contact between the Cu/NbN interface in our device, the superconducting gap Δ is suppressed close to the interface because of the superconducting proximity effect [48]. Thus in calculating $f_0(\Delta)$ we assume that Δ is spatially dependent as $\Delta(x) = \Delta_0 x/\xi$, where Δ_0 is the bulk gap of the NbN and ξ is the superconducting coherence length. We take $x = 0$ at the Cu/NbN interface and $x > 0$ in the NbN, with the x axis normal to the interface. We confirmed that the spatial evolution of Δ does not affect our final results drastically. As seen in Fig. 1(b), ρ_{xx} is almost constant for $T_{\rm C} < T < 20$ K, thus we take in this temperature range $\rho_{xx} = \rho_{xx}(T = 20\ {\rm K}) \equiv \rho_{\rm imp}$, and $\rho_{\rm qp} = \rho_{\rm imp}/[2f_0(\Delta)]$. Then the ratio of $\Delta R_{\rm ISHE}$ in the superconducting to the normal (at 20 K) states for a certain I becomes

$$\frac{\Delta R_{\rm ISHE}^{\rm super}}{\Delta R_{\rm ISHE}^{\rm normal}} = \left(\frac{I_{\rm s}^{\rm super}}{I_{\rm s}^{\rm normal}}\right)\frac{\zeta^{\rm super}}{\zeta^{\rm normal}}\left(\frac{a(\rho_{\rm imp}/2f_0(\Delta)) + b(\rho_{\rm imp}/2f_0(\Delta))^2}{a\rho_{\rm imp} + b\rho_{\rm imp}^2}\right)e^{-\frac{d}{\lambda_{\rm Q}}}. \tag{12}$$

The term $I_{\rm s}^{\rm super}/I_{\rm s}^{\rm normal}$ can be described as [40]

$$\frac{I_{\rm s}^{\rm super}}{I_{\rm s}^{\rm normal}} = \int_{-\infty}^{\infty} n_{\rm S}(E)\left(-\frac{\partial f_0(E)}{\partial E}\right)dE, \tag{13}$$

DOI: 10.1038/NMAT4276

where $n_S(E)$ is the density of the states of the NbN wire. We found from the temperature dependence of α_H and ρ_{xx}, $|b/a| \sim 10^6\ \Omega^{-1}\mathrm{cm}^{-1}$. Thus hereafter we only consider the term quadratic in ρ_{imp}. From the relation between I and T in Eq. (8), we performed calculation assuming $\Delta T(\equiv T - T_0) \propto \sqrt{I}$, and obtained the relation between $\Delta R_{ISHE}^{super}/\Delta R_{ISHE}^{normal}$ and I, as shown by the solid curve in Fig. 3b and Fig. 3c in the main text. In the analysis we used $\rho_{imp} = 220\ \mu\Omega$cm and $\zeta^{super}/\zeta^{normal} = 4$ taking into account higher resistivity of NbN than CuIr in [46]. We numerically calculated (12) and (13) at each x, and finally the results were averaged over x. We note that the calculation can reproduce well the experimental data in the small I regime ($I < 10\ \mu$A), but it fails when I is larger. This might stem from the difference between the relation $\Delta T \propto \sqrt{I}$ and that obtained from (8). The present model is not complete enough to explain the behavior of the inverse spin Hall signal in the whole I region. It is possible that effects other than the effective temperature increase also play a role, thus more elaborated models are necessary to reproduce all experimental data. Since as I increases, T also increases, the deviation of the theoretical calculations from the experimental data might be related to the anomalous temperature dependence of ΔR_{ISHE} close to T_C as we will discuss in the next section.

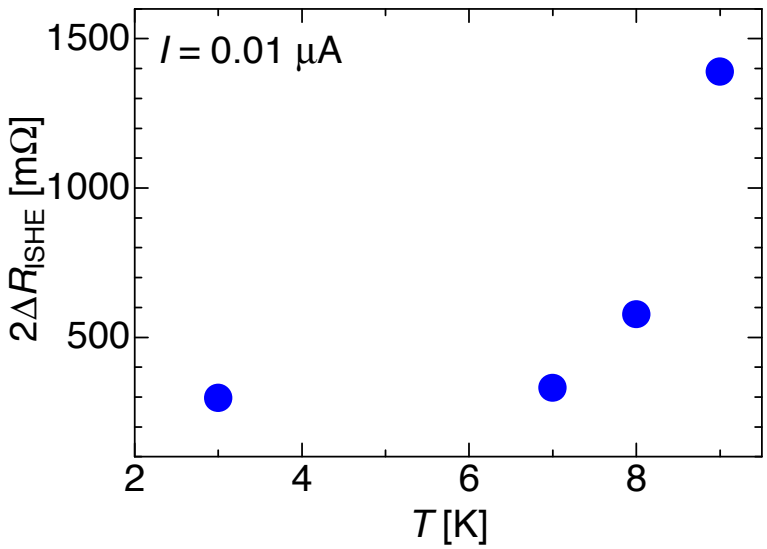

FIG. 4. Temperature dependence of the ISHE signal ($2\Delta R_{ISHE}$) below T_C.

S.5 TEMPERATURE DEPENDENCE OF THE ISHE SIGNALS

We finally show the temperature dependence of ΔR_{ISHE} below T_{C}. As T is approaching to T_{C}, we observed diverging ISHE signals, which are not taken into account in the previous theories [49, 50]. We note a strong resemblance between the charge imbalance (CI) effect and the inverse spin Hall signal near T_{C}. Therefore diversing ΔR_{ISHE} might be associated with the divergence of the CI at $T = T_{\mathrm{C}}$. However, it is also possible that nonequibrium superconductivity plays an important role [52]. For future studies, it is necessary to obtain a clear relation between the spin injection current and the temperature and also to elucidate the origin of this anomalous T dependence of the inverse spin Hall signals based on more experimental data and elaborate models.

S.6 BASELINE RESISTANCE IN THE ISHE SIGNALS

For the figures in the main text, the baseline resistance (backgrounds) is subtracted from the raw data. The baseline resistance in nonlocal setup is ideally zero, but it always appears in real measurements. Its origins are often discussed in many studies, and several possible candidates are proposed for nonlocal measurements with spin valves, such as current inhomogeneity at the ferromagnet/nonmagnet interface [53] or thermal effects [54]. However, none of them are conclusive and the origin of the baseline resistance is still an open question. The baseline resistance also appears in our measurements regardless of the NbN in the normal or superconducting state, and its magnitude and sign depend on devices. We note that the existence of the backgrounds does not affect the inverse spin Hall signals.

[31] Shoji, A., Kiryu, S. and Kohjiro, S. Superconducting properties and normal-state resistivity of single-crystal NbN films prepared by a reactive rf-magnetron sputtering method. Appl. Phys. Lett. **60**, 1624 (1992).

DOI: 10.1038/NMAT4276

[32] Karplus, R. and Luttinger, J. M. Hall effect in ferromagnetics. Phys. Rev. **95**, 1154 (1954).

[33] Nagaosa, N. *et al.* Anomalous Hall effect. Rev. Mod. Phys. **82**, 1539 (2010).

[34] Onoda, S., Sugimoto, N. and Nagaosa, N. Intrinsic versus extrinsic anomalous Hall effect in ferromagnets. Phys. Rev. Lett. **97**, 126602 (2006).

[35] Smit, J. The spontaneous Hall effect in ferromagnetics 1. Physica **21**, 877 (1955).
Smit, J. The spontaneous Hall effect in ferromagnetics 2. Physica **24**, 39 (1958).

[36] Berger, L. Side-jump mechanism for the Hall effect of ferromagnets. Phys. Rev. B **2**, 4559 (1970).

[37] Tian, Y., Ye, L. and Jin, X. Proper scaling of anomalous Hall effect. Phys. Rev. Lett. **103**, 087206 (2009).

[38] Pomeroy, J. M. and Grube, H. J. Negative resistanceh errors in four-point measurements of tunnel junctions and other crossed-wire devices. J. Appl. Phys. **105**, 094503 (2009).

[39] Moodera, J. S. *et al.* Geometrically enhanced magnetoresistance in ferromagnet-insulator-ferromagnet tunnel junctions. Appl. Phys. Lett. **69**, 708 (1996).

[40] Wakamura, T. *et al.* Spin injection into a superconductor with strong spin-orbit coupling. Phys. Rev. Lett. **112**, 036602 (2014).

[41] Henny, M. *et al.* 1/3-shot-noise suppression in diffusive nanowires. Phys. Rev. B **59**, 2871 (1999).

[42] Mallet, F. *et al.* Scaling of the low-temperature dephasing rate in Kondo systems. Phys. Rev. Lett. **97**, 226804 (2006).

[43] Cadden-Zimansky, P. and Chandrasekhar, V. Nonlocal correlations in normal-metal superconducting systems. Phys. Rev. Lett. **97**, 237003 (2006).

[44] Papaconstantpoulos, D. A., in *Handbook of the Band Structure of Elemental Solids* (Plenum, New York, 1986).

[45] Ashcroft, N. W. and Mermin, N. D. in *Solid State Physics* Ch2 (Saunders College, 1976).

[46] Niimi, Y. *et al.* Extrinsic spin Hall effect induced by iridium impurities in Cu. Phys. Rev. Lett. **106**, 126601 (2011).

[47] Takahashi, S., Yamashita, T., Imamura, H. and Maekawa, S. Spin-relaxation and magnetoresistance in FM/SC/FM tunnel junctions. J. Mag. Mag. Mater. **240**, 100 (2002).

[48] Buzdin, A. I. Proximity effects in superconductor-ferromagnet heterostructures. Rev. Mod. Phys. **77**, 935 (2005).

[49] Takahashi, S. and Maekawa, S. Spin Hall effect in superconductors. Jpn. J. Appl. Phys. **51**, 010110 (2012).

[50] Kontani, H., Goryo, J. and Hirashima, D. S. Intrinsic spin Hall effect in the s-wave superconducting state: analysis of the Rashba model. Phys. Rev. Lett. **102**, 086602 (2009).

[51] Mamin, H. J., Clarke, J. and Van Harlingen, D. J. Charge imbalance induced by a temperature gradient in superconducting aluminum. Phys. Rev. B **29**, 3881 (1984).

[52] Langenderg, D. N. and Larkin, A. in *Non-Equilibrium Superconductivity* (North-Holland, Amsterdam, 1980).

[53] Johnson, M and Silsbee, R. H. Calculation of nonlocal baseline resistance in a quasi-one-dimensional wire. Phys. Rev. B **76**, 153107 (2007).

[54] Bakker, F. L., Slachter A., Adam, J. -P and van Wees, B. J. Interplay of Peltier and Seebeck effects in nanoscale nonlocal spin valves. Phys. Rev. Lett. **105**, 136601 (2010).